HLSTM: Heterogeneous Long Short-Term Memory Network for Large-Scale InSAR Ground Subsidence Prediction

Qinghao Liu, Yonghong Zhang, Jujie Wei, Hongan Wu, and Min Deng

***Abstract*—Accurate prediction of ground subsidence is of great significance for the prevention and mitigation of this type of geological disaster. It is still a challenge when wide area is concerned. In this article, a heterogeneous long short-term memory (HLSTM) network is proposed for large-scale ground subsidence prediction based on interferometric synthetic aperture radar (InSAR) data. First, the study area is divided into homogeneous subregions through spatial clustering of InSAR-derived subsidence velocity. Second, a specific LSTM model is constructed to capture complex nonlinear temporal correlations embedded in InSAR-derived subsidence time series for each subregion. Essentially both spatial heterogeneity and temporal correlation are incorporated into the HLSTM prediction. In the experiment part, the HLSTM predictor is validated using a subsidence monitoring result from 80 Sentinel-1 images acquired over Cangzhou, China, from 2017 to 2019. The HLSTM result shows the highest prediction accuracy through comparisons with the results from other seven methods.**

***Index Terms*—Deep learning, heterogeneity, interferometric synthetic aperture radar (InSAR), long short-term memory (LSTM), subsidence prediction.**

I. Introduction

IN ORDER to meet the needs of rapid development of economy, many kinds of underground natural resources such as coal, petroleum, and groundwater have been extensively exploited. As a result, large-scale ground subsidence has taken place, which usually causes serious harm to the environment and human life [1], [2]. Therefore, high-precision prediction of ground subsidence is of great significance in the practice of taking actions of subsidence prevention. At present, most of the ground subsidence prediction methods rely on *in situ* data obtained by traditional surveying techniques [3], [4]. Although related technologies have high observation accuracy, some shortcomings severely restrict the development of large-scale, high-precision deformation predictions, such as low spatial density, high acquisition costs, long observation periods, etc. [5]. With the development of remote sensing technology, continuous large-area ground monitoring provides strong support for the prediction of ground subsidence.

In general, the existing prediction methods of ground subsidence can be divided into three categories: physical methods, statistical methods, and machine learning methods. The physical methods usually start from a physical model describing the subsidence mechanism, and then need to determine several physical parameters such as lithological and hydrological parameters through field testing and experiments, and finally predict the ground subsidence at a future moment. The researches on mining subsidence model [6], subway subsidence model [7], and groundwater coupling model [8] are within this category. However, it is usually difficult to know the physical parameters. The statistical method aims to establish a time-based mathematical function to predict subsidence. Fan and Zhang [9] and Li [10] outlined some typical statistical methods. Some scholars have also proposed methods that additionally consider spatial location to predict subsidence [11]–[14]. However, linear assumptions make it difficult for them to resolve the nonlinear relationship between spatiotemporal data. On the other hand, since the constitutive relationship of underground geotechnical medium is not considered, such methods are usually difficult to promote. Comparatively, machine learning methods are not restricted by the complex physical parameters, such as geology and hydrology. In addition, they do not require an interpretable relationship (e.g., interpretable mathematical formulas) to be formalized between independent and dependent variables. Existing methods such as support vector regression (SVR) [15], artificial neural network [16], Bayesian network [17], etc., have all been used in subsidence prediction. However, due to the difficulty of feature extraction or the difference in data granularity, the existing machine learning methods are usually difficult to obtain high prediction accuracy. Besides, a global model cannot handle well the variations in the relationship between the dependent variable and the independent variable in different regions, this leads to a common problem that the results lack interpretability.

In the realm of interferometric synthetic aperture radar (InSAR) time series prediction, many predictions based on hyperbolic model [18], probability integration method [19], support vector regression [20], recurrent neural network [21], and

Manuscript received May 1, 2021; revised June 27, 2021, July 27, 2021, and August 12, 2021; accepted August 15, 2021. Date of publication August 24, 2021; date of current version September 9, 2021. This work was supported by the National Key R&D Program of China under Grant 2017YFE0107100 and Grant 2018YFB0505400. (*Corresponding author: Yonghong Zhang.*)

Qinghao Liu is with the Chinese Academy of Surveying and Mapping, Beijing 100830, China, and also with the School of Geosciences and Info-Physics, Central South University, Changsha 410083, China (e-mail: 1580748414@qq.com).

Yonghong Zhang, Jujie Wei, and Hongan Wu are with the Chinese Academy of Surveying and Mapping, Beijing 100830, China (e-mail: yhzhang@casm.ac.cn; weijj@casm.ac.cn; wha_105@aliyun.com).

Min Deng is with the School of Geosciences and Info-Physics, Central South University, Changsha 410083, China (e-mail: dengmin028@yahoo.com).

Digital Object Identifier 10.1109/JSTARS.2021.3106666

other methods have been carried out. However, these works have ignored the fact that the statistical characteristics of subsidence driving factors will vary with geographic locations [9]. In fact, subsidence at any location can be attributed to these factors, such as geological structure, rainfall distribution, land use, etc. If the spatial heterogeneity of these factors is not well considered, the constructed prediction model may be invalid in local areas [22]. Deep learning methods can obtain valuable knowledge from InSAR time series about how those factors affect subsidence, but the spatial heterogeneity between them cannot be modeled by neural networks. Therefore, it is necessary to consider more reasonable strategies to predict subsidence.

In this article, the spatial heterogeneity between subsidence sequences is considered in the deep learning algorithm. This strategy learns different subsidence sequence patterns separately instead of constructing a globally unique model. Specifically, first, we use a time series clustering strategy to divide the study area into several InSAR homogeneous subregions; then, we construct long short-term memory (LSTM) models in parallel between different subregions to understand their subsidence patterns; finally, we verified the effectiveness of heterogeneous long short-term memory (HLSTM) from the perspective of error analysis and spatial pattern.

The main contributions of our work are as follows.

1) In order to handle the spatial heterogeneity of ground subsidence, the method of time series clustering is integrated into the data preparation process.
2) The HLSTM model is proposed, which can automatically learn the complex nonlinear subsidence patterns of heterogeneous regions.
3) The validity of HLSTM is verified from the perspective of error analysis and spatial pattern.

II. Methodology

In this section, we construct HLSTM in two steps. First, introduce how to use clustering to reduce spatial heterogeneity. Second, multiple deep learning networks are trained to fit the subsidence patterns in different subregions. Finally, Section II-C of this article explains the operation process of HLSTM.

A. Clustering to Handle Heterogeneity

If the spatial heterogeneity is ignored, the training of the neural network is usually insufficient and may affect the prediction performance [23]. There are three main methods to solve spatial heterogeneity: 1) Build a local model. 2) Transform/decompose the nonstationary data. 3) Space partition [24]. However, the complexity and quantity of time series limit the feasibility of the first two methods. According to the similarity and separation between time series, cluster analysis can divide the data set into different clusters to describe similar feature mapping (see Fig. 1). Therefore, the clustering strategy can be used to determine the spatial partition [25]. However, when it comes to large-volume, nonsignificantly aggregated spatiotemporal data, the proposed clustering methods [26]–[29] all face the following challenges, such as nonunique number of clusters, low efficiency, single partition shape, complex parameter settings, etc., which severely limit the application of InSAR ground subsidence partitioning. It has been found that the two-step strategy based on K-means [30] and Delaunay triangulation [31] can efficiently solve the partition problem. The two-step strategy (called KDP) considers not only the attribute distance between the object and the center of a certain category, but also the adjacency relationship between the object and the existing spatial object in the category by adjusting the side length constraint constant α. So, it can obtain reasonable partitioning results.

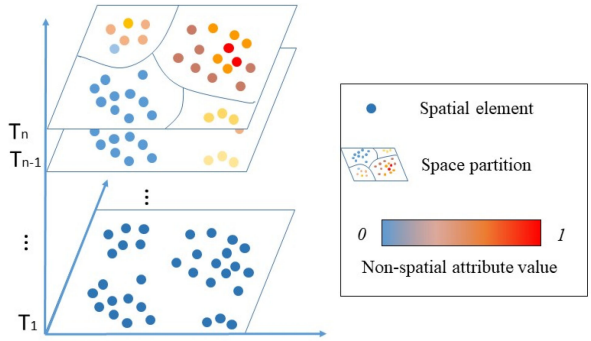

Fig. 1. Partition processing to handle spatial heterogeneity.

In this article, the Euclidean distance of the mean subsidence velocity is chosen as the similarity measure. The effectiveness of clustering results is evaluated by the Davies–Bouldin (DB) index [32]. Where S_i and S_j, respectively, represent the diameter of the clusters, d_{ij} represents the distance between the two clusters, and k represents the number of clusters. The smaller the DB index, the better the clustering effect

$$R_{ij} = \frac{S_i + S_j}{d_{ij}} \tag{1}$$

$$\mathrm{DB} = \frac{1}{k} \sum_{k}^{i=1} \max_{i \neq j} R_{ij}. \tag{2}$$

Clustering results with different cluster numbers k are obtained using K-means method, considering the mean subsidence velocity and Pearson correlation, respectively, to calculate the DB index, and the number of clusters meeting the metrics will be selected, and the further subregion division is based on Delaunay triangulation [31]. The KDP algorithm flow is described as follows:

Enter: $D(m,n)$, K, α
Output: $S\{subregion\ 1, \ldots, subregion\ p\}$
for each k in $2:K$
  get $K\_Clu\{clu\ 1, \ldots, clu\ k\}$ from $D(m,n)$ by k
  calculate DB
  evaluate K_Clu by DB
get the most suitable k with a smaller DB
for each clu in K_Clu
  get Delaunay triangulation
  constrain Delaunay triangulation by α
get $S\{subregion\ 1, \ldots, subregion\ p\}$

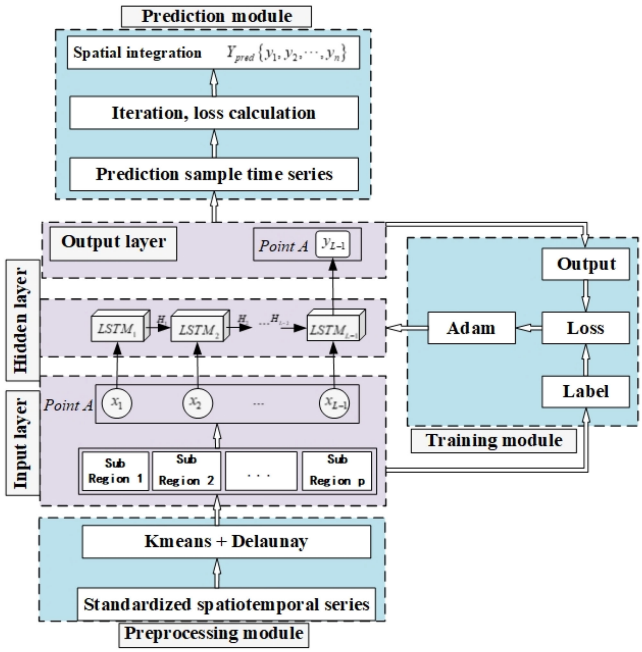

Fig. 2. HLSTM subsidence prediction framework.

where $D(m,n)$ represents the deformation space-time matrix, *m* and *n* represent the length of their time series and the number of space point targets; S represents the spatial partition result of point targets; K_Clu represents the result of K-means clustering. α represents the constraint parameter of the side length in the Delaunay triangulation network. If the side length is greater than the mean of all side lengths by more than α times the standard deviation, then this side is regarded as an abnormal connection and will be interrupted.

B. HLSTM Prediction Framework

As shown in Fig. 2, the main body of the prediction framework is composed of three modules, including clustering module, training module, and prediction module. Among them, the clustering module is responsible for heterogeneous processing of spatiotemporal data to meet network input requirements, the training module is designed to generate a pretrained model, and the prediction module is designed to run the model and obtain prediction results. The key to the entire framework is a deep neural network, including input layer, hidden layer, and output layer. Among them, the hidden layer is modeled by the LSTM model to learn the characteristics of each subsidence sequence, and the output layer is a collection of prediction results under different subregions. The input data of HLSTM is a matrix of geocoded subsidence sequences. In the clustering module, the mean subsidence velocity and the spatial distance between point targets need to be extracted from the input data. In the training module and the prediction module, the differential subsidence sequence needs to be extracted as samples.

In this article, we assume that some fixed-length sequences contain important deformation patterns, and record the subsidence sequence of each point target as $D_m = \{d_1, d_2, \ldots, d_m\}$. In order to accurately learn these deformation patterns, a training sample with an adjustable length of parameter L can be extracted and recorded as $D_{\text{train}} = \{d_{m-L}, d_{m-L+1}, \ldots, d_{m-1}\}$ in each subsidence sequence, where the last Y values of the sample are used as the sample label, and the first $L-Y$ values is used as the sample input, and it satisfies constraint $\{2 \le L < m, 1 \le Y < L\}$. Besides, the z-score standardization method is applied to each sample to reduce the negative impact of the deformation range on model training. An example of sample division is shown in Fig. 3. In addition, the length of the sample label can also be adjusted according to actual needs. According to this division method, n samples can be extracted from the entire deformation area. Specifically, the standardized sample data is divided into p clusters, and the local network model is used to learn the subsidence patterns under each subregion.

C. Model Details and Optimization

Heterogeneity processing and network training are the main content of running HLSTM models. Clustering can divide the study area into several deformation zones based on subsidence characteristics. Each deformation zone is further divided into several homogeneous subregions based on the Delaunay triangulation [31], and each subregion is used to build a local network model. Network training is a process of adjusting weights and biases until the user-defined stopping criteria are met. In this article, when the error-epoch curve of the training set and the test set are both converged, the pretrained model can be accepted. Generally, we used 30 epochs to train the target model. This process is mainly based on hidden layers and other connections.

When training the HLSTM prediction model, L, K, and S are the most critical network parameters, which, respectively, represent the length of the sequence, the number of network layers, and the number of features in each hidden layer. Generally, grid search strategy is used to optimize model parameters. Taking reducing the mean prediction error as the metric for parameter optimization. For each subregion, a random sampling of 70% of the sample sequences is enough to train a high-performance network, while considering the modeling time. The objective function can be expressed as

$$\min\varepsilon\ (Y_{\text{real}}, Y_{\text{pred}}) = |Y_{\text{real}} - Y_{\text{pred}}| \tag{3}$$

$$\text{s.t.} \begin{cases} 2 \le L < m, \text{step}_L \\ 2 \le K < i, \text{step}_K \\ 2 \le S < S_{\max}, \text{step}_S \\ L, K, S \in N \end{cases}. \tag{4}$$

In the formula, step_L, step_K, and step_S are the search steps of related parameters, respectively. Generally, the grid search range i and $S_{\max}$ need to be set by human experience based on the error convergence effect. In this article, the Adam [33] estimation algorithm is used as the training optimizer.

After the network training reaches the convergence requirement, the network prediction is performed. First, we intercept $D_{\text{pred}} = \{d_{m-L+1}, d_{m-L+2}, \ldots, d_m\}$ from the subsidence sequence of each point target as a prediction sample. And the accuracy of model training and prediction can be quantitatively

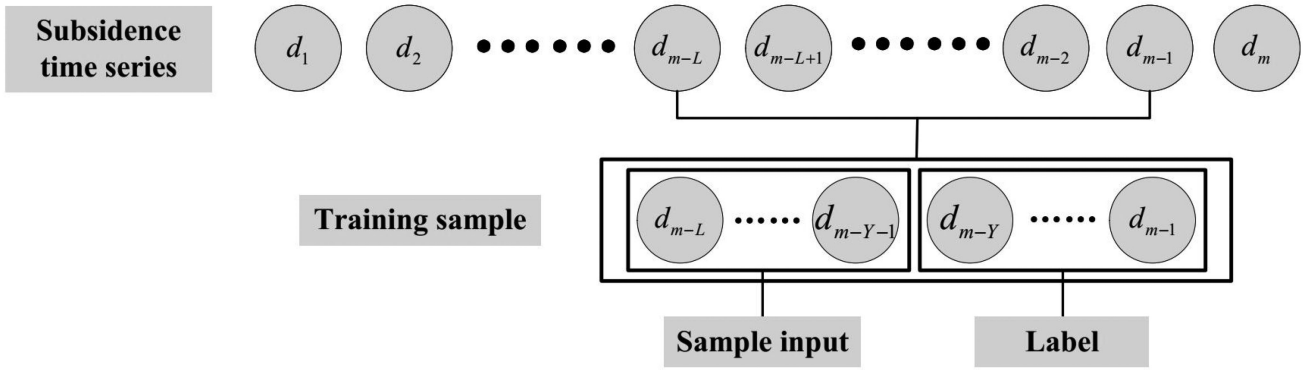

Fig. 3. Sample division in single subsidence sequence.

given as follows:

$$\mu = 100 * \left(1 - \frac{\mathrm{MAE}}{\mathrm{MAD}}\right)\% \tag{5}$$

$$\mathrm{MAE} = \frac{1}{n}\sum |Y_{\mathrm{real}} - Y_{\mathrm{pred}}| \tag{6}$$

$$\mathrm{MAD} = \frac{1}{n}\sum |Y_{\mathrm{real}}| \tag{7}$$

where μ represents the prediction accuracy of the model, MAE represents the mean absolute error, and MAD represents the mean actual deformation.

Overall, HLSTM is a predictor driven by InSAR data. Specifically, the training set and the test set are only used to train or adjust the pretraining model, and the time cost is much lower than the SAR image update cycle (usually 12 days). Furthermore, the subsidence at the *m*th moment can be predicted by the pretrained model, when the real subsidence data at the *m*th moment is updated, D_{pred} is immediately submitted to the pretrained model to update the model parameters. This means that we can use the latest observations to predict future subsidence in a short time.

III. Experiment Result Analysis

A. Dataset

The Cangzhou area of China [34] has experienced a maximum cumulative subsidence of at least 398 mm in the past 4 years. A test site is chosen in this area, and 80 Sentinel-1A images acquired between January 2017 to December 2019 were used as the data source. Furthermore, we use multiple Master-image Coherent Target Small-baseline Interferometric SAR method [35] to generate InSAR deformation time series (see Fig. 4). As a result, we obtained 430476 subsidence sequences derived from the same number of high-coherence points. Local linear interpolation is used to fill in the data at the missing moment, which is caused by poor coherence. As a result, each point target has 89 deformation data at equal time intervals. The accuracy verification results show that the root-mean-square error of the deformation inversion process is 7.2 mm.

In order to verify the effectiveness of HLSTM, we also generated a set of simulation data according to the actual characteristics of ground subsidence. First, we assume that there are some meaningful subsidence patterns derived from heterogeneous geographic environments. Then, using the sum of random values and trend items to simulate 5 subsidence patterns (see Fig. 5): stable pattern (blue), uniform uplift (yellow), uniform

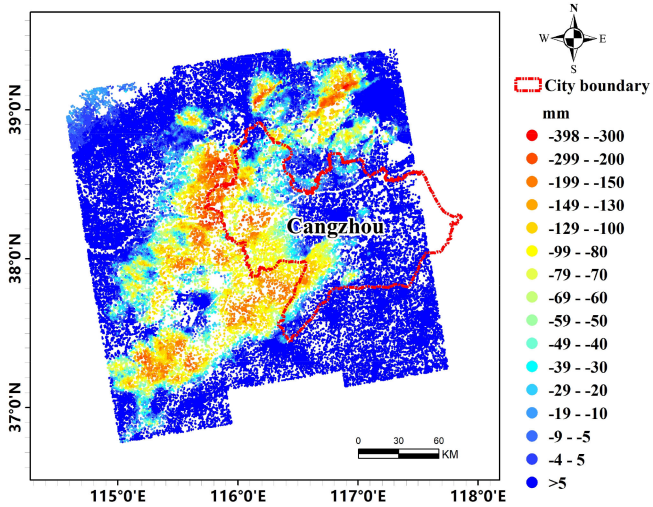

Fig. 4. Spatial distribution of cumulative deformation in Cangzhou area.

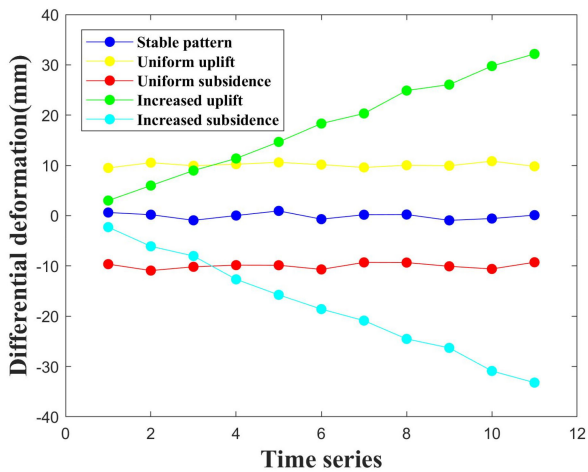

Fig. 5. Change of differential deformation with time series (random case).

TABLE I
COMPOSITION OF SIMULATED DIFFERENTIAL DATA

subsidence pattern	color	trend items	random values	time step	number
stable pattern	blue	0	(-1,1)	11	10,000
uniform uplift	yellow	Y=10X	(-1,1)	11	10,000
uniform subsidence	red	Y= -10X	(-1,1)	11	10,000
increased uplift	green	$Y= 1.5\ X^2 + 1.5X$	(-1,1)	11	10,000
increased subsidence	indigo	$Y=-1.5\ X^2 - 1.5X$	(-1,1)	11	10,000

subsidence (red), increased uplift (green), and increased subsidence (indigo). In total, 10 000 sequences are generated for each subsidence pattern, with a total time step of 11. The composition of the simulated differential data is shown in Table I. In fact, the simulated data of each subsidence pattern represents a preset spatially independent subregion.

B. Homogeneous Subregion Partition

In order to reduce the influence of spatial heterogeneity on subsidence prediction, the KDP algorithm is used to divide the real research area into several homogeneous subregions. The two-step clustering strategy only needs to set an additional side length constraint constant α ($\alpha = 3$ in this article) to obtain clusters with similar attributes and spatial proximity. When the number of clusters (usually less than 10) is 2, a smaller DB index can be obtained (see Fig. 6). The clustering results are further constrained into 6 homogeneous subregions by the method [31] (see Fig. 7). Each homogeneous subregion is a collection of highly coherent points with similar subsidence characteristics and adjacent spatial locations. This strategy not only describes the similarity of the deformation sequence, but also highly coincides with the spatial pattern of the deformation funnel (see Figs. 7 and 4). In addition, in Table II, the measurement results based on q-statistic [36] shows that partitioning effectively weakens the stratified heterogeneity in the study area. Therefore, the KDP algorithm can weaken the spatial heterogeneity of the subsidence mechanism well.

C. Network Parameter Analysis

First, we analyzed the impact of the sample label length on the prediction effect. The MAE heatmap (see Fig. 8) shows that as the increase of the sample label length (SLL), the model error under different sample input lengths (SIL) also increases. The color bars indicate the range of MAE values in each grid. It is also important that although the error difference is small, it can be clearly found in the vertical direction that the length of the sample input is not always a significant linear trend. Therefore, the findings in the heat map inspired us to set the SLL to 1.

Second, we analyzed the prediction effect under different network parameters. In Fig. 9, the error results under different parameter settings (SIL and SLL) show that the model prediction accuracy is not always positively correlated with the model complexity, but there is a better combination locally. When the grid search range is determined, the distribution of the optimal parameters tends to be consistent. For example, when SIL $=$ 60 and SLL $= 1$, the optimal parameters always focus on "the number of network layers is 3, and the number of neurons is 10.

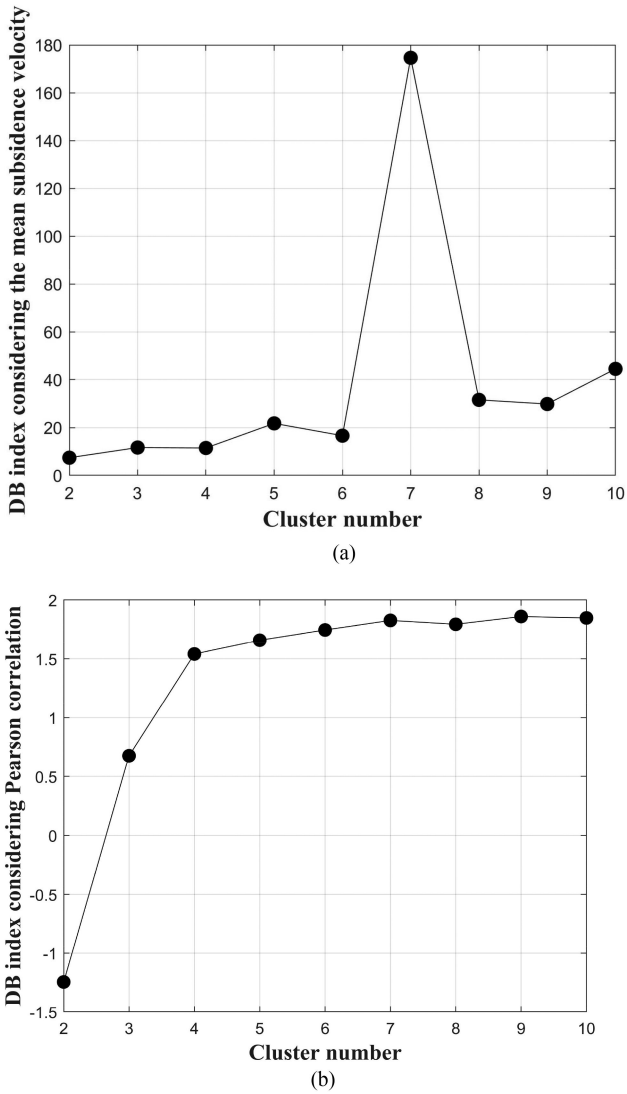

Fig. 6. Evaluation indexes changes with different cluster numbers. (a) DB index considering the mean subsidence velocity. (b) DB index considering Pearson correlation.

Third, we further analyzed the prediction results of subregions under different sample input lengths. As shown in Fig. 9, the blue subregions 1–3 are divided by zone 2 and the red subregions 4–5 are divided by zone 1, the black noise point polyline represents a collection of isolated points and smaller clusters. Fig. 10 suggests that after the SIL reaches a certain level, the minimum prediction error of different subregions gradually increases. This means that the prediction effect does not always improve as SIL increases. Besides, although some subregions are in the

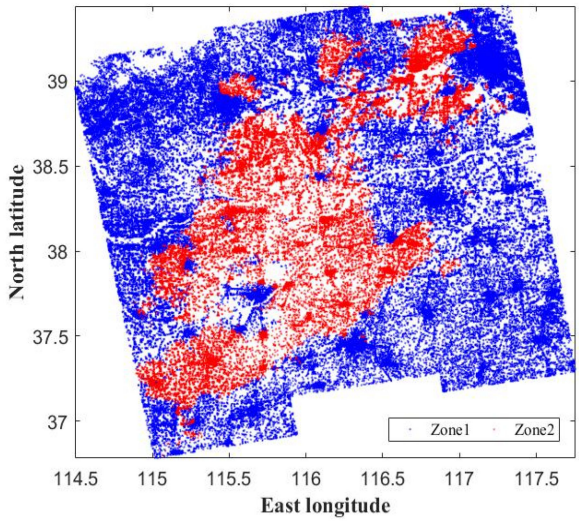

(a)

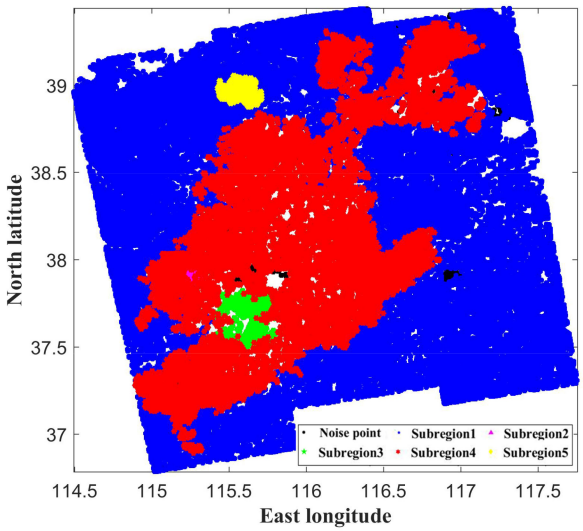

(b)

Fig. 7. Division of homogeneous subregions based on KDP algorithm. (a) Initial space partition results (2 deformation zones). (b) Final space partition results (6 subregions).

TABLE II
SIGNIFICANT CHANGES IN HETEROGENEITY AFTER PARTITIONING

Status	Area name	q	p (0.05)	Significance
Initially	Global	0.5061	0	Yes
Partitioned	Subregion1	0	0.9072	No
	Subregion2	0.0337	0.0741	No
	Subregion3	0.0051	0.4804	No
	Subregion4	0.0002	0.6241	No
	Subregion5	0	0.9865	No
	Noise point	0.0055	0.4651	No

same level of deformation zone, the difference of geographical environment makes it produce different deformation patterns (For example, the first 3 subregions constrained by zone 2 have different optimal SILs), which means that it is necessary to consider spatial constraints when dividing subregions. It should be noted that when it comes to small-scale ground subsidence,

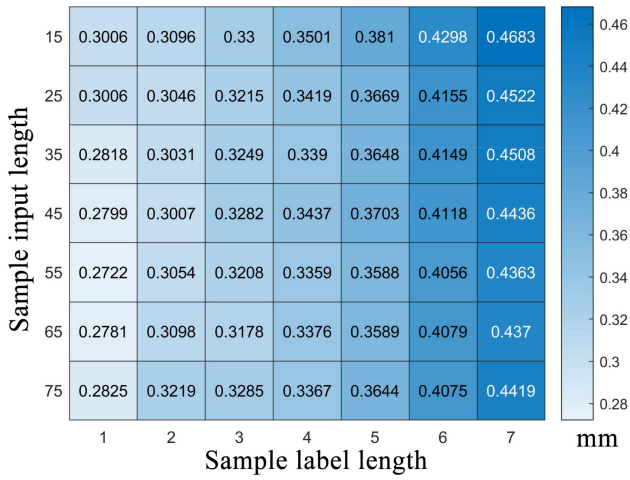

Fig. 8. Grid search results of MAE (K = 30, S = 2).

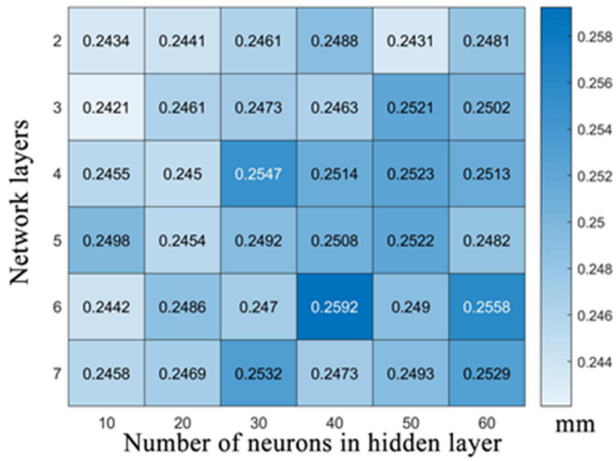

Fig. 9. Optimal combination of network parameters in grid search results (SIL = 60, SLL = 1).

training a well-fitted neural network will become difficult, and the performance of HLSTM will be affected by the volume of data. As shown in Fig. 9, suboptimal models are usually trained based on smaller subregions or noise point data. Therefore, we merge clusters with a number of point targets less than 1000 into a set of noise points.

As shown in Fig. 11(a), in order to compare the mean absolute error of the deformation zone 1-2, the subregion errors are merged, which is a weighted strategy based on the number of point targets. Fig. 11(a) shows the results of the two deformation zones based on the merger of the subregions, it shows that there is a slight difference in the optimal training sample length: 87 periods and 78 periods, which indicates the most relevant duration of ground subsidence, and each period represents 12 days. This difference can be attributed to the long-term deformation patterns obtained by the InSAR time series, in addition, the long-term correlations of the subsidence information in different geographic environments (homogeneous regions) are different [see Fig. 11(b)]. Therefore, blindly inputting a longer deformation sequence introduces a certain noise error.

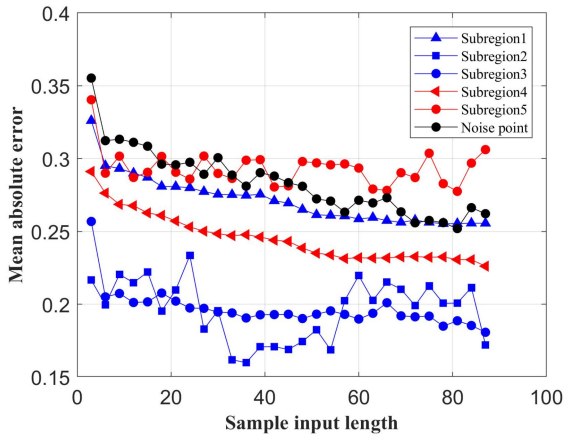

Fig. 10. Relationship between SIL and MAE under subregions.

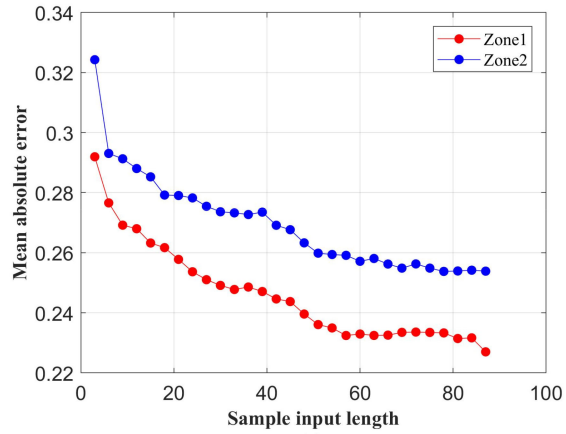

(a)

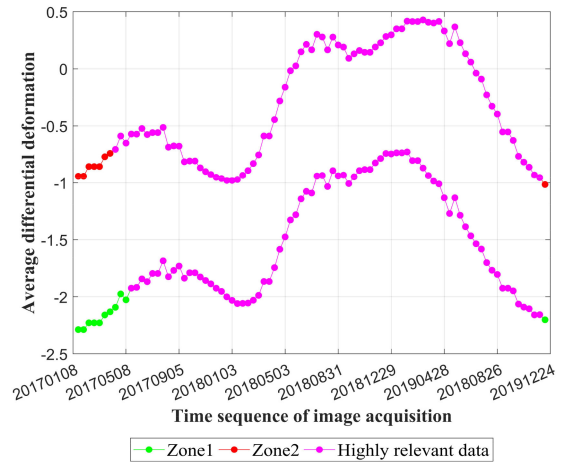

(b)

Fig. 11. Analysis on the optimal SIL. (a) Error analysis. (b) Visualization of highly relevant data.

D. Performance Comparison

We compared the HLSTM model with other seven methods, the modeling time (including preprocessing) and prediction error are selected as evaluation indicators, and all benchmark methods use the same data source.

TABLE III
COMPARISON OF EXPERIMENTAL RESULTS OF DIFFERENT PREDICTION MODELS

Model		Error			Accuracy	Time/h or s
		MAE/mm	SD/mm	MSE/mm^2		
SES[10]		0.5417	1.4868	3.2499	37.7%	23s
ARIMA[13]		0.3612	0.3202	0.2329	58.6%	518h
STARIMA[14]		0.2991	0.2711	0.1629	65.6%	610h
MLR[10]		0.4473	0.3582	0.3284	48.6%	450s
SVR[18]		0.2675	0.2676	0.1431	66.1%	241s
RNN[3]		0.2846	0.2699	0.1539	69.3%	367s
LSTM[21]		0.2543	0.2493	0.1268	70.8%	226s
HLSTM	Zone1	0.2523	0.2492	0.1257	71.1%	173s
	Zone2	0.2471	0.2404	0.1189		56s
	Global	0.2511	0.2472	0.1242		191s

MAE: mean absolute error; **SD**: standard deviation; **MSE**: mean square error.

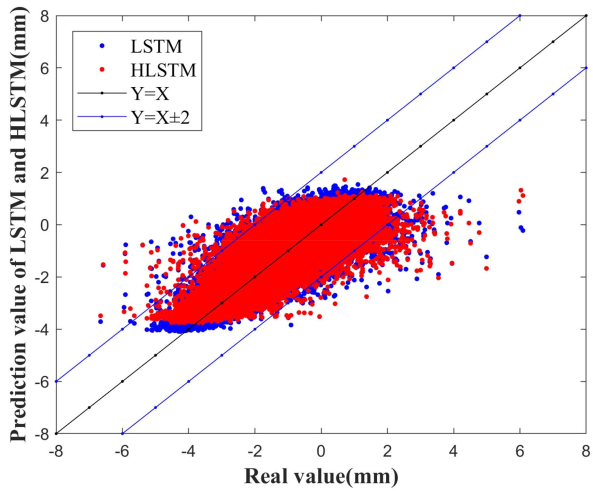

Fig. 12. Comparison of error distribution between HLSTM and LSTM.

It can be seen from Table III that compared to other algorithms, LSTM and HLSTM have better performance. The autoregressive integrated moving average (ARIMA) model and the space-time ARIMA (STARIMA) model need to be constructed once for each point target. Therefore, they are not suitable for large-scale ground subsidence prediction. In Table III, the modeling time of these two methods is the estimated value of sampling. The experimental results reflect: 1) When predicting subsidence, the deep learning network designed for time series prediction is better than typical statistical methods and machine learning methods. 2) Long-term dependence does have an impact on the prediction of ground subsidence (compare RNN and LSTM). 3) The newly proposed spatial heterogeneous processing strategy increases the prediction accuracy of LSTM by 0.3% and get a more homogeneous absolute error distribution (compare HLSTM and LSTM). Fig. 12 shows that the red point target (HLSTM) is closer to the $Y = X$ line than the blue point target (LSTM) under the same truth value. Obviously, HLSTM has a certain inhibitory effect on the overall variance of the point target prediction results, especially as the real deformation increases, this improvement will be more significant. 4) The proposed HLSTM obtains the lowest MAE and MSE, which proves the effectiveness of the proposed method.

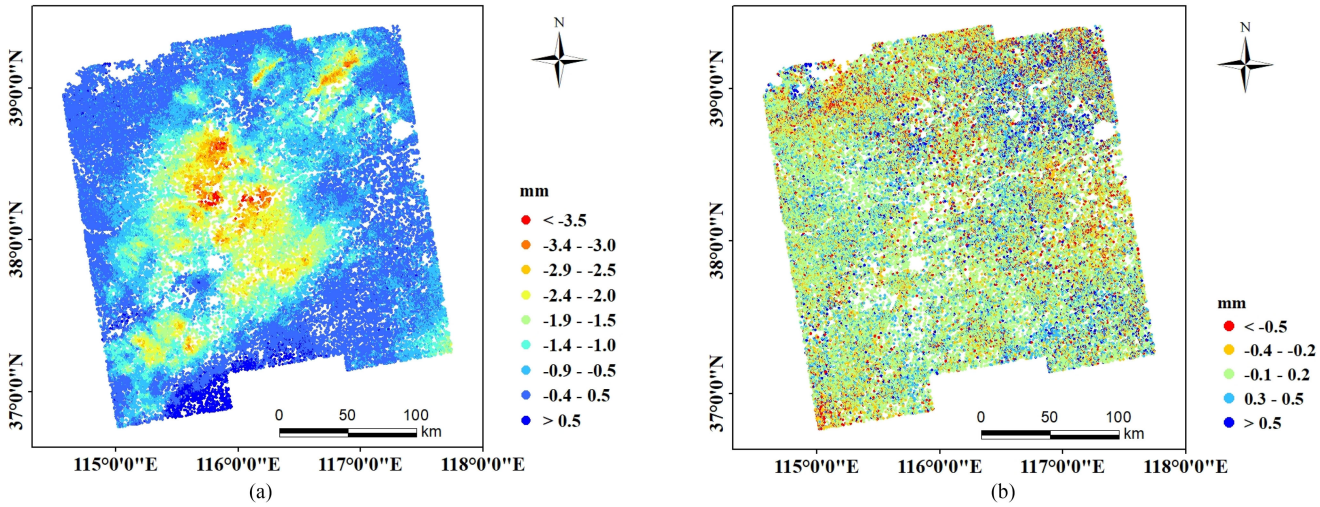

Fig. 13. Prediction results of differential deformation in Cangzhou. (a) Differential deformation prediction results. (b) Error distribution of differential deformation prediction.

TABLE IV
PERFORMANCE COMPARISON OF HLSTM AND LSTM MODELS

Model		Parameter	MAE/mm	SD/mm	Accuracy	Time/s
LSTM		L=5, K=2, S=25	1.2945	1.2962	92.16%	19.82
HLSTM	Subregion1	L=4, K=2, S=25	0.2481	0.1441		7.47
	Subregion2	L=4, K=2, S=5	0.2501	0.1444		7.18
	Subregion3	L=3, K=2, S=5	0.2497	0.1448		7.39
	Subregion4	L=4, K=2, S=5	0.2512	0.1458		6.54
	Subregion5	L=5 K=3, S=5	0.2498	0.1438		7.20
	Global		0.2494	0.1443	98.49%	6.54

In order to further prove that the advantages of HLSTM over LSTM do exist, we retrained the model based on simulated data. The results in Table IV show that the strategy of spatial predivision to weaken spatial heterogeneity significantly improves the prediction accuracy and time efficiency. Therefore, the prediction results of this set of simulation data further prove the advantages of the HLSTM model.

It should be noted that the significance of this improvement will also be affected by the subsidence data, especially the subsidence patterns of different research areas and the revisit period of the SAR satellites. For example, in general, samples with a larger differential deformation value (with a faster subsidence velocity or lower time resolution) will get a larger relative error under the same termination training criterion. This is why the real data in Cangzhou area has not improved more significantly than simulated data. In fact, how to determine the best time resolution to extract the deformation pattern is still a challenge, and we will propose our multiscale modeling strategy in another work.

E. Spatial Analysis

Fig. 13 shows the results of our prediction of subsidence in Cangzhou from the scale of the entire image. Combined with the large-scale representation of the real deformation, it can be found that our prediction results are highly consistent with the real deformation, the subsidence funnel is clearly displayed, and 85.2% of the point target prediction errors are within ± 0.5 mm. The running results of HLSTM show that among the 430476-point targets, the largest difference (cumulative) deformation prediction error is 8.75 mm, and the mean prediction accuracy reaches 71.1%. Because HLSTM trains each subregion independently, the main modeling time in Cangzhou area is consumed in the clustering module (18 s) and subregion 4 (173 s).

InSAR time series analysis provides an important reference for revealing the macroscopic ground subsidence patterns and evolution laws [5], but the prediction result of a single high coherence point is not significant. In order to explore the effectiveness of our prediction model, we use ArcGIS and other tools to compare and analyze the spatial statistical characteristics of the prediction results and real subsidence information. For the characteristics of spatial autocorrelation, hierarchical heterogeneity, and spatial pattern existing between the prediction results, the classic indicators *Moran's I, Getis* G^*, $\mathrm{q}-\mathrm{statistic}$, NNI, etc., are used to measure them separately. The results show that our prediction results did not significantly change the spatial statistical characteristics of real subsidence. That is to say, the deformation pattern of the original InSAR inversion result is still maintained, which spatially ensures the feasibility of the deep learning method in ground subsidence prediction. The detailed results of the spatial analysis are shown in Table V.

TABLE V
ANALYSIS OF SPATIAL CHARACTERISTICS OF TIME SERIES PREDICTION RESULT

Spatial characteristics	Metrics	Real image	Predicted image	Change analysis
Global spatial autocorrelation	$Moran's\ I$	$p = 0 < 0.05, z = 2055$	$p = 0 < 0.05, z = 2411$	Consistent
Local spatial autocorrelation	$Getis\ G^*$	Distinct cold and hot spots	Distinct cold and hot spots	Consistent
Stratified heterogeneity	$\mathrm{q-statistic}$	$p = 0 < 0.05, q = 0.5216$	$p = 0 < 0.05, q = 0.5219$	Consistent
Point pattern	NNI	$R = 0.45 < 1$	$R = 0.45 < 1$	Identical

IV. CONCLUSION

In this article, by constructing the HLSTM network model, the spatial heterogeneity is integrated into the field of ground subsidence prediction, and large-scale subsidence prediction is realized with high precision and time efficiency. The experimental results show that as follows.

1) The accuracy and processing time are marginally improved compared to classic deep learning approaches (RNN and LSTM).
2) The subsidence prediction method based on HLSTM can effectively maintain the spatial pattern of ground subsidence. And the effectiveness of the method is verified by comparing the spatial analysis metrics.
3) Using subsidence sequences to predict ground subsidence can avoid difficulties in obtaining hydrological data. Compared with other physical methods and machine learning methods, HLSTM has higher prediction accuracy without relevant data.

Although the pretrained model of this research is only applicable to the Cangzhou area, HLSTM can be extended to any large-scale, monitorable deformation area. This article is a prediction attempt driven by InSAR data. Some error sources in the InSAR results will inevitably affect the actual prediction performance of ground subsidence. In addition, the spatial heterogeneity of ground subsidence will change over time, and how to accurately capture geographic similarity is a problem worthy of research. In further work, we will implement a subsidence prediction method that considers more driving factors.

REFERENCES

[1] H. Su and Z. Hu, "A review of land subsidence research abroad," *Land Resour. Shanghai*, no. 2, pp. 65–77, 1980.

[2] R. Hu, Z. Yue, L. Wang, and S. Wang, "Review on current status and challenging issues of land subsidence in China," *Eng. Geol.,* vol. 76, no. 1/2, pp. 65–77, 2004.

[3] Q. Zhou, H. Shen, J. Zhao, and X. Xiong, "Tunnel settlement prediction by transfer learning," *J. ICT Res. Appl.*, vol. 13, no. 2, pp. 118–132, 2019.

[4] M. Hu, W. Li, K. Yan, J. Z, and H. Hu, "Modern machine learning techniques for univariate tunnel settlement forecasting: A comparative study," *Math. Problems Eng.*, vol. 2019, no. 1, pp. 1–12, 2019.

[5] J. Zhu, Z. Li, and J. Hu, "Research progress and methods of InSAR for deformation monitoring," *Acta Geodaetica et Cartographica Sinica*, vol. 10, no. 1, pp. 1717–1733, 2017.

[6] Z. Wang and K. Deng, "Richards model for prediction of dynamic surface subsidence in mining area," *Geotechnical Mechanics*, vol. 32, no. 6, pp. 1664–1668, 2011.

[7] C. Yuan, Z. Luo, S. Liu, G. Li, and L. Li, "Analysis and prediction of ground surface settlement caused by tunnel excavation in Qingdao area," *J. Rock Mechanics Eng.*, vol. 33, no. 0z2, pp. 4014–4019, 2014.

[8] C. Mi *et al.*, "Imaging land subsidence induced by groundwater extraction in Beijing (China) using satellite radar interferometry," *Remote Sens.*, vol. 8, no. 6, 2016, Art. no. 468.

[9] Z. Fan and Y. Zhang, "Application of intelligent algorithm in land subsidence prediction," *Surveying Mapping Spatial Geographic Inf.*, vol. 42, no. 5, pp. 183–188, 2019.

[10] L. Li, "Land subsidence prediction model and its application," *Chang'an Univ.*, vol. 71, pp. 1181–1194, 2014.

[11] H. P. A. B. T. and A. S. A. L., "Prediction maps of land subsidence caused by groundwater exploitation in Hanoi, Vietnam," *Resour.-Efficient Technol.*, vol. 1, no. 2, pp. 80–89, 2015.

[12] L. Anselin, J. L. Gallo, and H. Jayet, "Spatial panel econometrics," in *Springer Berlin Heidelberg*. Dordrecht, The Netherlands: Springer, 2008.

[13] D. A. Griffith, "Modeling spatio-temporal relationships: Retrospect and prospect," *J. Geographical Syst.*, vol. 12, no. 2, pp. 111–123, 2010.

[14] P. E. Pfeifer and S. J. Deutrch, "A three-stage iterative procedure for space-time modeling Phillip," *Technometrics*, vol. 22, no. 1, pp. 35–47, 1980.

[15] I. Ocak and S. E. Seker, "Calculation of surface settlements caused by EPBM tunneling using artificial neural network, SVM, and Gaussian processes," *Environmental Earth Sci.*, vol. 70, no. 3, pp. 1263–1276, 2013.

[16] W. Yinghua and X. Chang, "Using genetic artificial neural network to model dam monitoring data," in *Proc. 2nd Int. Conf. Comput. Model. Simul.*, 2010, pp. 3–7.

[17] M. A. Shahin, H. R. Maier, and M. B. Jaksa, "Settlement prediction of shallow foundations on granular soils using B-Spline neurofuzzy models," *Comput. Geotechnics*, vol. 30, no. 8, pp. 637–647, 2003.

[18] S. Kim, S. Wdowinski, T. H. Dixon, F. Amelung, and J. Won, "Measurements and predictions of subsidence induced by soil consolidation using persistent scatterer InSAR and a hyperbolic model," *Geophysical Res. Lett.*, vol. 37, no. 5, pp. 87–105, 2010.

[19] X. Wang, Y. Zhang, X. Jiang, and P. Zhang, "A dynamic prediction method of deep mining subsidence combines D-InSAR technique," *Procedia Environmental Sci.*, vol. 10, no. 1, pp. 2533–2539, 2011.

[20] B. Chen and K. Deng, "Integration of D-InSAR technology and PSO-SVR algorithm for time series monitoring and dynamic prediction of coal mining subsidence," *Surv. Rev.*, vol. 46, no. 339, pp. 392–400, 2015.

[21] Q. Liu *et al.*, "Time series prediction method of large-scale surface subsidence based on deep learning," *J. Surveying Mapping*, vol. 50, no. 3, pp. 396–404, 2021.

[22] M. Deng *et al.*, "Heterogeneous space–time artificial neural networks for space–time series prediction," *Trans. GIS*, vol. 22, no. 1, pp. 183–201, 2018.

[23] T. Cheng and J. Wang, "Accommodating spatial associations in DRNN for space–time analysis," *Comput. Environ. Urban Syst.*, vol. 33, no. 6, pp. 409–418, 2009.

[24] C. Brunsdon, "Local models for spatial analysis," *Int. J. Geographical Info Sci.*, vol. 23, no. 3/4, pp. 547–548, 2009.

[25] M. Deng, "Spatial point entity clustering algorithm," in *Spatial Clustering Analysis and its Application*. 1st ed. China: Sci. Pre, 2011, ch. 5, sec.10, pp. 133-134.

[26] J. Sander, M. Ester, H. P. Kriegel, and X. Xu, "Density-based clustering in spatial databases: The algorithm GDBSCAN and its applications," *Data Mining Knowl. Discov.*, vol. 2, no. 2, pp. 169–194, 1998.

[27] F. Bacao, V. Lobo, and M. Painho, "The self-organizing map, the Geo-SOM, and relevant variants for geosciences," *Comput. Geosciences*, vol. 31, no. 2, pp. 155–163, 2005.

[28] G. Li, M. Deng, and T. Cheng, "A spatial clustering method based on double distance," *J. Surveying Mapping*, vol. 37, no. 4, pp. 482–488, 2008.

[29] Y. Shi, Q. Liu, M. Deng, and X. Lin, "Hybrid spatial clustering method based on graph theory and density," *Proc. China Geographic Inf. Ind. Assoc.*, vol. 37, no. 11, pp. 1276–1280, 2012.

[30] X. Wu *et al.*, "Top 10 algorithms in data mining," *Knowl. Inf. Syst.*, vol. 14, no. 1, pp. 1–37, 2008.

[31] C.-R. Lin, K.-H. Liu, and M.-S. Chen, "Dual clustering: Integrating data clustering over optimization and constraint domains," *IEEE Trans. Know. Data Eng.*, vol. 17, no. 5, pp. 628–637, May 2005.

[32] D. L. Davies and D. W. Bouldin, "A cluster separation measure," *IEEE Trans. Pattern Anal. Mach. Intell.*, vol. PAMI-1, no. 2, pp. 224–227, Apr. 1979.
[33] D. Kingma and J. Ba, "Adam: A method for stochastic optimization," *Comput. Sci.*, vol. 1412, pp. 69-80, 2014.
[34] H. Zhou *et al.*, "Monitoring of recent ground surface subsidence in the cangzhou region by the use of the InSAR time-series technique with multi-orbit sentinel-1 TOPS imagery," *Int. J. Remote Sens.*, vol. 39, no. 21/22, pp. 8113–8128, 2018.
[35] Y. Zhang, B. Liu, H. Wu, X. Cheng, and Y. Kang, "Ground subsidence in xiong'an new area from 2012 to 2016 monitored by InSAR technique," *J. Earth Sci. Environ.*, vol. 40, no. 5, pp. 452–462, 2018.
[36] J. Wang, T. Zhang, and B. Fu, "A measure of spatial stratified heterogeneity," *Ecological Indicators*, vol. 67, no. 1, pp. 250–256, 2016.

Qinghao Liu received the master's degree from Central South University, Changsha, China, in 2021.

He is currently works with the National Basic Geographic Information Center from Central South University. Form 2019–2021, he was with the Chinese Academy of Surveying and Mapping as a guest graduate student and carried out a series of ground subsidence monitoring and prediction studies. He is currently working toward for the Ph.D. entrance examination. His research interests include spatial planning and spatiotemporal data mining.

Yonghong Zhang received the Ph.D. degree in photogrammetry and remote sensing from Wuhan University, Wuhan, China, in June 2001.

Since July 2001, he has been working with the Chinese Academy of Surveying and Mapping. From May 2002 to December 2003, he was engaged in Postdoctoral Research with the Geography Department of King's College London, U.K. His research interests include synthetic aperture radar interference and polarization measurement technology and application, disaster monitoring, change monitoring, etc., and has presided over the completion of more than 40 national, provincial, and ministerial scientific research projects.

Jujie Wei received the Ph.D. degree in photogrammetry and remote sensing from Wuhan University, Wuhan, China, in 2014.

From July 2015 to June 2017, he was engaged in Postdoctoral Research with the Chinese Academy of Surveying and Mapping. Since June 2017, he has been with the Chinese Academy of Surveying and Mapping. His current research interests include remote sensing (including synthetic aperture radar and optical) image interpretation, multitemporal remote sensing image change detection, and the application of deep learning in remote sensing image understanding.

Hongan Wu received the Ph.D. degree in cartography and geographic information systems from the Institute of Remote Sensing Applications, Chinese Academy of Sciences, Beijing, China, in 2009.

Since 2009, he has been with Chinese Academy of Surveying and Mapping, where he is currently an Associate Researcher. His research interests include the high-precision ground deformation monitoring theory, technology and application of multipass satellite synthetic aperture radar interferometry, such as large-area deformation monitoring, and safety monitoring of infrastructures and buildings.

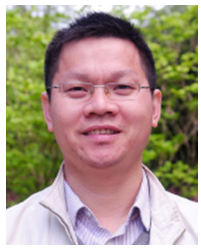

Min Deng received the Ph.D. degrees in cartography and geographic information engineering from Wuhan University, Wuhan, China, in 2003 and the Asian Institute of Technology, Khlong Nueng, Thailand, in 2004.

He is currently the head of the Department of Geo-Information and the Doctoral Supervisor with the School of Geosciences and Info-Physics, Central South University, Changsha, China. He ever hosted numerous major projects including a Key project of National Natural Science Foundation of China. His current research interests include coordinated planning, spatio temporal data mining, and spatiotemporal analysis and modeling.